Amplitude and Frequency Modulation With an On-Chip Graphene-Based Plasmonic Terahertz Nanogenerator

Justin Crabb, Xavier Cantos-Roman, *Student Member, IEEE*, Gregory R. Aizin, and Josep M. Jornet, *Senior Member, IEEE*

***Abstract*—Terahertz communication is envisioned as a key technology not only for the next generation of macro-scale networks (e.g., 6G), but also for transformative networking applications at the nanoscale (e.g., wireless nanosensor networks and wireless networks on chip). In this paper, an on-chip THz nano-generator with amplitude and frequency modulation capabilities is presented. The proposed device uses and leverages the tunability of the Dyakonov-Shur instability for the growth and modulation of plasmonic oscillations in the two-dimensional electron gas channel of a graphene-based high-electron-mobility transistor. An in-house developed finite-element-methods platform, which self-consistently solves the hydrodynamic model and Maxwell's equations, is utilized to provide extensive numerical results demonstrating the device's functionality along with ultra-wide bandwidth and high modulation index capabilities.**

***Index Terms*—Graphene transistor, Dyakonov-Shur instability, THz modulation, plasmonics.**

I. Introduction

As TODAY'S cutting-edge technology pushes forward, we see an increased demand for faster connectivity between a growing number of users. This implies higher data rates in the Tera-bits-per-second (Tbps) range, requiring drastically higher bandwidths that can be achieved in the terahertz (THz) domain (0.1–10 THz) of the electromagnetic (EM) spectrum. Applications that would benefit from such high-data-rate wireless networks, to name a few, include wireless network-on-chip (WNoC) [1], the Internet of Nano-Things [2], and wireless nanosensor networks [3]. For example, the benefits of using THz WNoCs is the reduced propagation delay which is practically zero at the chip-scale compared to wired interconnects [4], the flexibility and reconfigurability of logical topology without physical modification, and, consequently, improved latency, throughput, and energy consumption [5].

Currently there are three main approaches for THz signal generation, namely, electronic, photonic, and plasmonic. In the electronic approach, recently reviewed in [6], silicon- and III-V semiconductor-based devices such as resonant tunneling diodes (RTDs) [7] and heterojunction bipolar transistor-based feedback oscillators [8] are used. These structures commonly require cryogenic temperatures for high frequency operation, suffer parasitic capacitances and resistances, and resonate at a fixed frequency. Since this frequency is often below the THz threshold, additional step-up devices include chains of frequency-multipliers [9] such as Schottky diodes, often suffering major power degradation and low conversion efficiencies. These electronic devices operate in the lower-THz region. Alternatively, the photonic approach utilizes optical and optoelectronic devices to step down to THz frequencies, with a large variety of designs having a wide range of operating principles [10], [11]. Some examples are Quantum Cascade Lasers (QCLs) [12], [13], heterodyne/photomixing structures [14], and laser-driven sources [15]. However, these designs are often bulky, possess low efficiency and output power, require cryogenic temperatures, and offer minimal tunability.

Many of today's advances in operations with THz signals are based on the plasmonic approach [16], [17], [18], [19], [20], [21], [22], [23], [24] due to its promise of compact THz devices with room temperature operation, high tunability, and low power consumption. In this approach, charge density waves (plasmons) of THz frequency are excited in the two-dimensional (2D) electron channel of semiconductor- or graphene-based high electron mobility field-effect transistors (FET), and are used for THz EM signal generation, amplification, and detection. The FET's channel serves as a resonant plasmonic cavity, supporting sustained plasmonic oscillations in the THz range [18], [19], and is tunable by external voltage and/or current sources.

Various FET designs have been proposed for on-chip THz devices, retaining the plasmonic oscillations within the 2D channel [20]. The plasmonic nature of the FET THz oscillator allows its confinement within the channel, miniaturizing the THz generator to a few microns, compared to passive THz antennas on the order of hundreds of microns. The THz EM signal is generated when sustained plasma oscillations are maintained in the FET plasmonic cavity. As shown in the seminal work

Manuscript received 31 March 2022; revised 3 August 2022; accepted 16 September 2022. Date of publication 20 September 2022; date of current version 28 September 2022. This work was supported in part by the Air Force Office of Scientific Research under Grant FA9550-16-1-0188, and in part by the US National Science Foundation under Grant CNS-2011411. The review of this article was arranged by guest editors of the Special Issue for NanoCoCoA2021. *(Corresponding author: Justin Crabb.)*

Justin Crabb, Xavier Cantos-Roman, and Josep M. Jornet are with the Department of Electrical and Computer Engineering, Institute for the Wireless Internet of Things, Northeastern University, Boston, MA 02115 USA (e-mail: crabb.j@northeastern.edu; cantosroman.x@northeastern.edu; jmjornet@northeastern.edu).

Gregory R. Aizin is with the Kingsborough College and the Graduate Center of the City University of New York, New York, NY 10016 USA (e-mail: Gregory.Aizin@kbcc.cuny.edu).

Digital Object Identifier 10.1109/TNANO.2022.3208084

by Dyakonov and Shur [25], it becomes possible if certain asymmetric boundary conditions are imposed at the opposite ends of the plasmonic cavity – the so-called Dyakonov-Shur (DS) regime. The FETs in the DS regime are fed by outside circuitry, supplying an energy necessary for sustained plasma resonance in the channel and radiated THz EM wave. Numerical investigations of THz emission from the high electron mobility transistors (HEMTs) in [21], [22], [23], [26] show that hundreds of nanowatts of radiated power are possible. A III-V semiconductor based HEMT in the DS regime is numerically modeled in [23], and a graphene HEMT in the DS regime is considered in [26]. Further improvement in the THz FET operation is connected with micro patterning the gate. The periodic grating gate [24], [27], [28], [29] inserts additional periodicity into the gated resonant cavities along the channel and enhance the efficiency of the device by strengthening the coupling between the plasmonic oscillations and the EM field. The grating gates can also serve as antennas, converting plasmonic oscillations into THz EM radiation.

In addition to THz EM signal generation, modulation is required for the integration of information in signal communications. Currently there are two main approaches for the modulation of THz signals. The first involves pulse-based THz signals, e.g., time-spread on-off keying (TS-OOK) where femtosecond-long pulses represent symbols [30]. The second approach uses carrier wave modulation. Various device configurations and techniques for THz carrier-wave modulation have been investigated and developed [31]. This includes amplitude modulators [32] that are usually limited to a few hundred MHz, and phase modulators [33] that can be readily incorporated into plasmonic devices. Recent progress in THz amplitude and phase modulation is mostly based on the use of externally controlled reflection/transmission of the incident THz EM wave in layered structures with various tunable metasurfaces [34], [35]. Modulation depths up to 87% with 0.7 THz bandwidth were reported [34]. Recent review of the THz modulators with tunable metasurfaces can be found in [36]. Some progress in the THz frequency modulators had also been reported [37] but it remains extremely limited, removing an important additional degree of freedom from today's THz communication systems. Moreover, the majority of available devices for THz modulation are not integrated on chip with other elements of the THz transmitter, and they require an external THz EM source. Recently the RTD-based on-chip THz transmitters with modulating capabilities have been reported [38]. They demonstrate the room temperature operation with modulation frequency up to few tens of GHz and the carrier frequency in the sub-THz range [39] though the RTD-based emitters with the fundamental frequencies as high as 2 THz have been reported [38].

In this paper, we present a tunable plasmonic THz nanogenerator based on a graphene HEMT with amplitude and frequency modulation (AM & FM) capabilities, offering ultrahigh AM and FM bandwidth at room temperature operation. The advantage of using graphene as a 2D electron channel in HEMT is due to its extremely high electron mobility at room temperature [40], [41], as well as excellent optical and electrical tuning capabilities. The device is numerically modeled in our in-house developed multiphysics simulation platform allowing simultaneous self-consistent solution of the hydrodynamic and Maxwell's equations, describing the device operation [26]. The simple design allows the integration of the modulator into the THz generator via direct tuning of the device parameters. We report our theoretical results showing bandwidths up to several hundred GHz and modulation depths exceeding 40%.

Our very early studies of this problem had been presented in the proceedings of the ACM NanoCom 2021 conference [42]. Here, in continuation of this work, we discuss in detail the physical effects leading to amplitude and frequency modulation and determine theoretical limits of the modulation bandwidths confirmed by the direct numerical experiment. Also, we present the modulation results and metrics directly as a function of the transistor tuning input signals, such as the source-drain current and the gate voltage. We then use common binary shift keying modulation schemes to demonstrate device performance for practical applications.

The device applications are envisioned in WNoCs, where today's proposed schemes mostly include graphene nano-antennas [43], requiring a signal generator and modulator in addition to the micron-scale components. Replacing the system components with our single proposed device allows a more compact device architecture. Furthermore, the compact size of the device when compared to larger THz antennas with external sources makes it attractive for use in nanomachines, such as nanosensor networks.

The remainder of this paper is organized as follows. In Section II we discuss the device architecture, and its principles of operation for THz signal generation and modulation. Section III overviews the multiphysics simulation platform used to model the device. The simulation results are presented in Section IV, where we demonstrate successful amplitude and frequency modulation and analyze the device performance metrics. Finally, we present our conclusions in Section V.

II. Modulator Device Structure and Principles of Operation

In this section the basic design of the graphene-based plasmonic HEMT is presented, and the working principles of the generator and the modulator are discussed.

A. Device Structure

The proposed HEMT device is shown in Fig. 1 and consists of a graphene channel sitting atop a dielectric substrate. The graphene channel is separated from the metal gate with a dielectric barrier, while the metal source and drain contacts lie on either side of the channel. The gate voltage V_{gs} applied between the source and the gate contacts defines the 2D electron density n_0 in the graphene layer, and the bias current I_{ds} between the source and drain contacts defines the electron drift velocity v_0 in the graphene channel with electron flow density in the channel $j_0 = n_0 v_0$. In our numerical simulations we choose geometrical parameters commonly used in the graphene HEMTs with the channel length $L = 1\,\mu\mathrm{m}$, the dielectric barrier thickness $d = 20\,\mathrm{nm}$, and the substrate thickness $l = 400\,\mathrm{nm}$. We used the

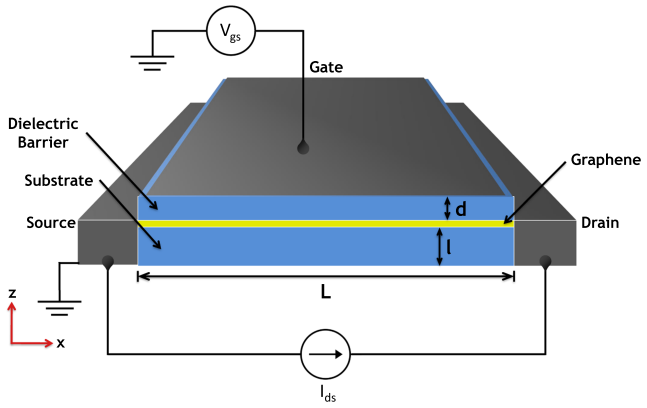

Fig. 1. Schematic of the proposed graphene transistor structure.

electric permittivity of the dielectric material $\epsilon = 3.8$, and also assumed that all HEMT contacts have a very large conductivity, making them practically ideal metal contacts at THz frequencies.

B. Dyakonov-Shur Instability

In 1993, Dyakonov and Shur theoretically demonstrated [25] that electron plasma instability is developed in the plasmonic cavity formed in the 2D electron channel of the high-mobility FET biased by the DC current, provided that the asymmetric boundary conditions are imposed at the opposite ends of the cavity. In particular, when electron flow is directed from the source to the drain, the AC impedance between the gate and the drain (Z_{gd}) must be larger than the same impedance between the gate and source (Z_{gs}): $Z_{gd} \gg Z_{gs}$. Given the capacitive nature of these impedances, the asymmetric conditions can be realized experimentally by depleting the electron channel near the drain in the FET saturation regime [44] or by asymmetric positioning of the gate with respect to the source and drain contacts [45]. In the ideal limit of $Z_{gs} = 0$ and $Z_{gd} = \infty$, these boundary conditions are equivalent to the conditions $n(x = 0, t) = n_0$ and $j(x = L, t) = j_0$, where functions $n(x, t)$ and $j(x, t)$ describe spatio-temporal evolution of the electron density n and electron flow density j in the channel with the source and drain contacts positioned at $x = 0$ and $x = L$ respectively, see Fig. 1.

As shown in [25], under these conditions, random fluctuations of the electron or current density traveling downstream increase in amplitude after reflection from the drain contact whereas the same fluctuation traveling upstream does not change its amplitude after reflection from the source contact. As a result of multiple reflections, the amplitude of plasma fluctuations increases exponentially with characteristic time determined by the electron transit time through the channel L/v_0. This exponential growth is impeded by the damping effect due to random electron scattering described by the electron momentum relaxation time τ. If $L/v_0 > \tau$, the instability is developed in the uniform electron plasma. For graphene structures, the instability increment γ is determined as [26], [46]

$$\gamma = \frac{v_0}{2\,L} - \frac{1}{2\tau}. \tag{1}$$

Growth of plasma fluctuations is accompanied by increasing heating and radiation losses. When the energy supplied by the external circuit is balanced by the losses, the electron system in the channel stabilizes in some stationary state. Numerical studies of graphene transistors in the DS regime [26], [47] demonstrated that the instability endpoint represents a coherent (nonchaotic) anharmonic oscillator with the electron density and plasmonic current periodically changing in time with fundamental frequency

$$f_0 = \frac{v_p}{4\,L}, \tag{2}$$

where

$$v_p = \sqrt{\frac{v_F^2}{2} + \frac{e^2\sqrt{n_0}dv_F}{\sqrt{\pi}\epsilon\hbar}} \tag{3}$$

is the plasma wave velocity in the gated 2D graphene channel and $v_F = 1.5 \times 10^6$ m s^{-1} is the Fermi velocity in graphene. This frequency coincides with the frequency of the quarter-wavelength standing wave in the plasmonic cavity. Sustained plasma oscillations in the graphene channel fed by the DC bias current emit EM waves at THz frequencies, thus the graphene HEMT in the DS regime represents the nano-generator of THz EM radiation. Simple estimates of the total emitted power made within 2D radiation model in [26] yield the power values on the order of tens of nanowatts. To enhance the radiation from the device, an antenna structure is needed. For example, graphene-based nano-antennas have been proposed in the literature [48], [49], [50], [51]. However, attaching the antenna structure to our device may significantly modify the DS boundary conditions reducing or even destroying the plasma instability. An alternative approach is to use the THz nano-generator as a feeding point of a half free-space wavelength metallic patch antenna by placing the graphene HEMT near or within the antenna resonant cavity [52]. The design of the resonant cavity and the placement of the feeding point within or near the cavity to maximize the radiation of the resulting structure is part of the ongoing work, and the results will be published elsewhere [53].

C. Integrated Modulator

The THz EM signal generated by the asymmetric graphene HEMT in the DS regime has constant frequency determined by (2) and (3) and constant amplitude. The addition of a temporal variance in the applied gate voltage or DC bias current results in a change of frequency or amplitude of the generated signal. This additional degree of freedom incorporates information into the signal, adding easy on-chip modulation capabilities to the THz nano-generator. This integrated generator/modulator system operating at room temperature with modulation capabilities limited only by the quality of the graphene 2D channel compares favorably with today's cutting-edge THz plasmonic modulators.

Amplitude modulation can be realized by varying the DC bias current passing through the transistor channel. This procedure changes the equilibrium drift velocity v_0 and the instability increment γ given by (1). An increased (decreased) instability increment leads to the stabilization of the plasma oscillations

with larger (smaller) amplitude, resulting in amplitude modulation of the THz EM signal.

Frequency modulation can be achieved by varying the gate voltage V_{gs} connected to the equilibrium electron density n_0 in the channel as

$$en_0 = C(V_{gs} - V_{th}), \tag{4}$$

where e is the elementary charge, $C = \frac{\epsilon\epsilon_0}{d}$ is the gate-to-channel capacitance per unit area, and V_{th} is the transistor threshold voltage. Varying the electron density n_0 changes the carrier frequency in (2) and (3), providing frequency modulation of the THz EM signal. Thus, applying even simple waveforms to the voltage and/or current sources can result in complex modulation schemes.

In Section III we consider tuning the equilibrium parameters via simple modulation schemes: $n_0(t) = n_0(1 + A_m \sin 2\pi f_m t)$ and $j_0(t) = j_0(1 + A_m \sin 2\pi f_m t)$, where f_m is the modulation frequency and A_m is the modulation amplitude. The simple waveform is then replaced with a binary sequence to demonstrate the device performance when using binary amplitude-shift keying and binary frequency-shift keying modulation schemes. We numerically analyze the results of applying these waveforms to our device, demonstrating the potential for ultra-broadband wireless communications.

III. Multi-Physics Modeling

While analytical formulas describe the DS instability in the linear regime, robust numerical solver is required to simulate the THz transistor performance in the radiating stationary state. Analysis of this performance requires a self-consistent solution of both the hydrodynamic equations and Maxwell's equations. The hydrodynamic equations model electron transport within the transistor channel, and Maxwell's equations describe the EM field in the surrounding space. These two sets of equations are used in our multi-physics simulation platform for accurate modeling of the proposed THz nano-generator. Here we describe the main building blocks of our numerical platform.

In the numerical simulations we restrict our consideration to the 2D spatial model, assuming that all variables are changing in the x-z plane only where the x-axis is chosen in the source-to-drain direction, and the z-axis is perpendicular to the 2D channel plane. Thus, the system is assumed to be uniform in the y-direction. The gridspace is set in the x-z plane with spatial increments dx and dz satisfying the Debye criterion [22] and the time increment dt limited by the Nyquist theorem: $dt < dx/2c$, where c is the speed of light.

A. Hydrodynamic Equations

The hydrodynamic equations describing 2D electron transport in graphene are the equation of continuity and the Euler equation. The continuity equation connecting the electron density $n(x,t)$ and the particle flow density $j(x,t)$ represents the conservation of the number of particles,

$$\frac{\partial n}{\partial t} = -\frac{\partial j}{\partial x}, \tag{5}$$

whereas the Euler equation describes the dynamics of the electron fluid. The non-linear Euler equation for the 2D electron fluid in graphene applicable at arbitrary values of the flow density j was derived in [26] and can be written in terms of n and j as

$$\begin{aligned}
&\frac{2-\beta^2(x,t)}{2}\frac{\partial j(x,t)}{\partial t} + v_F\beta(x,t)\frac{\partial j(x,t)}{\partial x} \\
&+ \frac{v_F^2}{2}\left(1-2\beta^2(x,t)\right)\frac{\partial n(x,t)}{\partial x} \\
&+ \frac{v_F\left(1-\beta^2(x,t)\right)^{5/4}}{\sqrt{\pi}\hbar}\sqrt{n(x,t)}eE_x(x,t) \\
&+ \frac{\left(j(x,t) - n(x,t)\frac{j_0}{n_0}\right)\left(1-\beta^2(x,t)\right)^{5/4}}{\tau}\sqrt{\frac{n_0}{n(x,t)}} = 0,
\end{aligned} \tag{6}$$

where $\beta(x,t) = \frac{j(x,t)}{v_F n(x,t)}$ and $E_x(x,t)$ is the induced AC electric field in the graphene channel. This equation includes the effects of random electron scattering in the relaxation time approximation. The "hydrodynamic block" of the numerical platform has two variables: the electron density n and the particle flow density j. The continuity equation is used to update the value of n and the Euler equation to update the value of j in each iteration.

B. Maxwell's Equations

The value of $E_x(x,t)$ in (6) is found from the system of Maxwell's equations

$$\begin{aligned}
\nabla \times \boldsymbol{E} &= -\mu_0\frac{\partial \boldsymbol{H}}{\partial t}, \\
\nabla \times \boldsymbol{H} &= -e(j-j_0)\delta(z)\hat{\mathbf{x}} + \epsilon\epsilon_0\frac{\partial \boldsymbol{E}}{\partial t},
\end{aligned} \tag{7}$$

where $\boldsymbol{E} = E_x\hat{\mathbf{x}} + E_z\hat{\mathbf{z}}$ and $\boldsymbol{H} = H_y\hat{\mathbf{y}}$ are the electric and magnetic components of the THz EM field induced by the electric current with density $-e(j-j_0)$ in the 2D graphene channel. A modified version of the finite-difference time-domain method [54] allows the implementation of all equations into a unified numerical computation platform which permits the overlap of the hydrodynamic and EM parameters for the conjunction of the two solvers when two sets of equations are looped for self-consistency. The numerical solver is run on MATLAB as commercial tools do not allow the simultaneous time-domain simulation of both solvers using the FDTD method. Further details of the numerical method can be found in [23]

IV. Numerical Results

In this section we present the results of our numerical simulations demonstrating the modulation capabilities of the proposed THz nanogenerator. This generator without modulation was considered in [26]. In Figure 2, we present the spatial distribution of the electric field component of the THz EM field radiated by the graphene HEMT shown in Fig. 1 assuming the electron density 3.8×10^{16} m^{-2} in the channel and the DC bias current density 23 A cm^{-1}. These results were obtained based

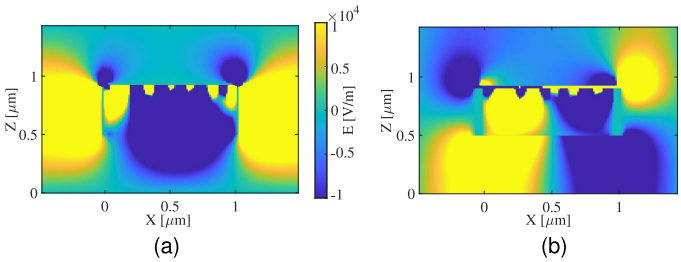

Fig. 2. Spatial distribution of the electric field components E_x (a) and E_z (b) of the THz EM radiation generated by the graphene transistor structure in the DS instability regime.

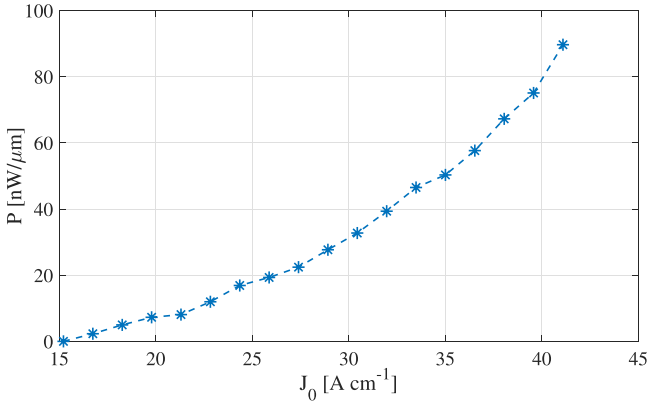

Fig. 3. Power radiated from the device P as a function of applied DC current density J_0 at constant electron density $n_0 = 3.8 \times 10^{16}$ m^{-2}.

on the approach developed in [26]. In the current 2D version of our simulation platform, we can solve the hydrodynamic and Maxwell's equations in two dimensions only, and therefore only E_x and E_z components are shown in Fig. 2. The same limitations allow us to find the radiated EM power P in the $x-z$ plane only, and the device with modulation considered in this section is thus demonstrated with the 2D power density P. The total 3D power can be roughly estimated by multiplying the power P by the width of the device in the y-direction. However, this estimate can only be viewed as the lower bound for the emitted EM power because the width of the considered graphene HEMT is much smaller than the wavelength of the THz EM radiation in free space. In this case, the dipole-like radiation is expected with the total power proportional to at least the squared device width.

A. Amplitude Modulation

Amplitude modulation of the THz EM signal can be achieved by varying the DC bias current density $J_0 = ej_0$ because the signal amplitude depends on J_0 as discussed in Section II. This conclusion is illustrated in Fig. 3 where we plot dependence of the radiated power P of the THz EM signal on the current density J_0. All numerical simulations were performed at constant electron density $n_0 = 3.8 \times 10^{16}$ m^{-2} and electron momentum relaxation time $\tau = 5$ ps. The radiated power increases with J_0 as expected, yielding the responsivity defined as $\frac{\Delta P}{\Delta J_0}$ around 35 μW A^{-1}.

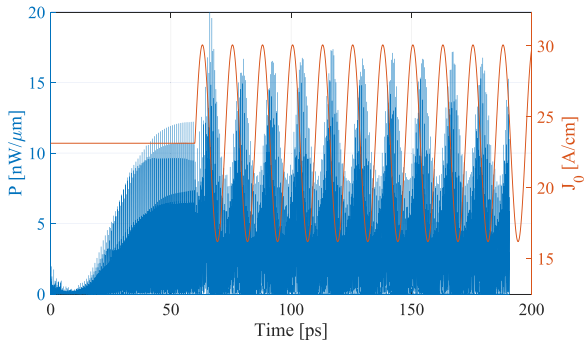

Fig. 4. Radiated power P (blue) as a function of time at bias current density $J_0(t) = J_0(1 + A_M \sin 2\pi f_m t)$ (orange) with $J_0 = 23$ A cm^{-1}, $f_M = 80$ GHz, and $A_M = 30\%$.

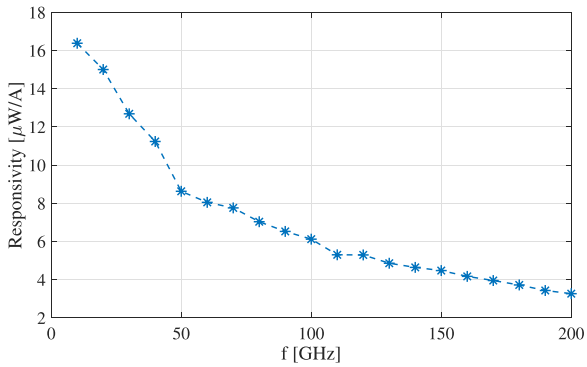

Fig. 5. Calculated responsivity of the AM signal as a function of modulation frequency f_m.

In Fig. 4 we present the results of our numerical simulations of the temporal evolution of the same signal when the bias current is modulated as $J_0(t) = J_0(1 + A_m \sin 2\pi f_m t)$. In this simulation, we used $J_0 = 23$ A cm^{-1}, the modulation frequency $f_m = 80$ GHz, and the modulation amplitude $A_m = 30\%$. The carrier frequency f_c defined in (2) and (3) is equal to 1.17 THz for our set of transistor parameters. The results shown in Fig. 4 demonstrate the amplitude modulation of the THz EM signal with responsivity around 6.75 μW A^{-1}. We note that the stable THz EM signal is set in the transistor after the transient time of $\sim$50 ps, thus the modulator was turned on at 60 ps mark. This transient time is determined by the inverse instability increment $1/\gamma$ and the amplitude of the stable THz signal. The same transient process causes the shift between the applied modulating signal (orange line in Fig. 4) and the resulting modulated THz EM signal (blue line in Fig. 4). However, the "shifting" time is notably shorter than the transient time because of the smaller change in the signal amplitude. Both the transient and the shifting time can be shortened by increasing the bias current J_0 and the instability increment. The finite "shifting" time effectively reduces the responsivity of the device. This effect becomes more pronounced at larger modulation frequencies. In Fig. 5 we plot the responsivity calculated in the dynamic regime as a function of the modulation frequency f_m illustrating this conclusion.

The finite shifting time limits the modulation bandwidth and degrades the performance of the amplitude modulator by

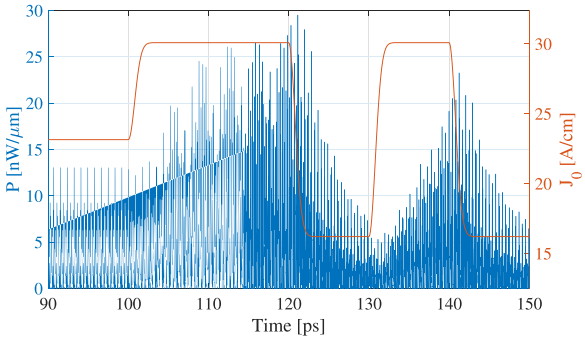

Fig. 6. Radiated power P (blue) as a function of time at bias current density $J_0(t)$ (orange) encoded with information bits $M = [11010]$ with symbol period $T_S = 10$ ps.

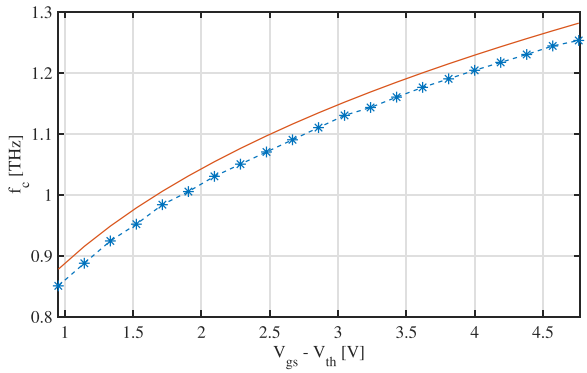

Fig. 7. Carrier frequency dependence on the gate voltage $V_{gs} - V_{th}$ found from (2) and (3) (orange line) and by direct numerical simulations (blue dots) at constant electron drift velocity $v_0 = 4 \times 10^5$ m s^{-1}.

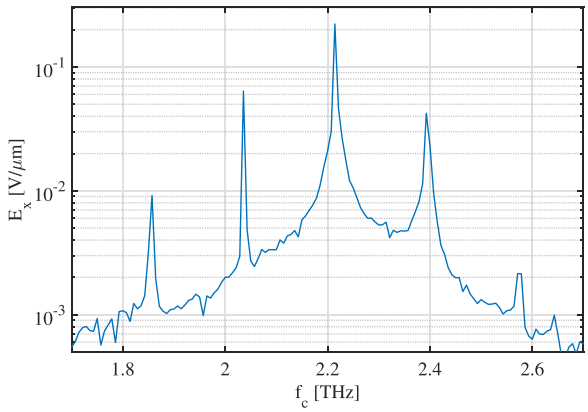

Fig. 8. Frequency spectrum of the THz EM signal in the presence of the modulating gate voltage signal with $f_M = 180$ GHz and $A_M = 30\%$.

reducing the modulation depth. The modulation bandwidth can roughly be estimated as γ, and for our set of device parameters is equal to $\sim$100 GHz at $J_0 = 23$ A cm^{-1}. This is the sole modulation frequency limit imposed by the physical processes in the graphene HEMT, though it can be further reduced due to frequency limitations in the external circuitry providing the modulation signal. In Fig. 4, the modulation depth is about 40% though the values exceeding 75% were obtained when f_m is decreased to 50 GHz and below. These values can be further increased at larger A_m.

Figure 6 shows the amplitude modulated signal when the sine wave (equivalent to [10101]) is replaced with information bits $M = [11010]$. In this Figure, the applied current (orange line) has a high value corresponding to bit '1' and a low value corresponding to bit '0'. The blue line shows the resulting THz EM signal amplitude modulated with the bits M. Here the information is encoded in the signal with a symbol period of $T_S = 10$ ps. This period corresponds to a modulating frequency of $f_m = 100$ GHz in our previous sine wave demonstration. The modulation bandwidth and modulation depth were calculated as 100 GHz and 60%, respectively, with an amplitude deviation of 9 nW μm^{-1}.

B. Frequency Modulation

Frequency modulation is based on the dependence of the carrier frequency f_c on the electron density n_0 controlled by the gate voltage V_{gs} applied to the transistor structure, as follows from (2)–(4). In Fig. 7, we show dependence of the carrier frequency f_c on the gate voltage V_{gs} (blue dashed line with asterisks) obtained by direct numerical simulation. In this simulation, we assumed that a constant electron drift velocity $v_0 = 4 \times 10^5$ m s^{-1} is maintained in the graphene channel by applied constant source-drain voltage. For comparison, we also show dependence of the fundamental plasma frequency f_0 on the gate voltage found analytically from (2)–(4) (orange solid line). The responsivity defined as $\frac{\Delta f_c}{\Delta V_{gs}}$, determined from the plot in Fig. 7, gradually decreases with increasing electron density changing from 200 GHz V^{-1} to 43.1 GHz V^{-1} when n_0 increases from 1×10^{16} m^{-2} to 5×10^{16} m^{-2}, corresponding to the gate voltage swing of 3.8 V.

The frequency spectrum of the generated FM modulated THz EM signal with $f_m = 180$ GHz, $A_m = 30\%$, and $n_0 = 3.1 \times 10^{16}$ m^{-2} is shown in Fig. 8. At this value of electron density, the fundamental plasma frequency $f_0 = 1.11$ THz. In our numerical simulations presented in Fig. 8, we used the second harmonic corresponding to the carrier frequency $f_c = 2f_0 = 2.22$ THz. The numerical results demonstrate a modulation bandwidth of 360 GHz, and the responsivity around 105 GHz V^{-1}. The modulation depth given by the ratio of frequency deviance to the carrier frequency is 8%.

In the case of frequency modulation, the value of the modulation frequency is limited only by the inverse electron relaxation time $1/\tau$ (the Drude roll-off frequency) as long as the plasma oscillations satisfy the ballistic limit condition: $2\pi f_c \tau \gg 1$ [55]. For $\tau = 5$ ps used in our calculations, it gives theoretical limit for the modulation frequency at 200 GHz, which can be reduced by the high frequency limitations of the external circuitry. Further analysis of the device operation shows successful FM capabilities up to and including this Drude roll-off frequency and substantial reduction in spectrum clarity above this limit.

Figure 9 shows the frequency modulated THz signal when the sine wave is replaced with information bits $M = [10010]$. Here the symbol period is $T_S = 5$ ps and the amplitude is $A_M = 30\%$. In this Figure, the frequency spectrum near the carrier frequency is shown at several consecutive moments of time with T_S increments. When the signal has a resonant frequency of $f_c = 2.34$ THz it is encoded with bit '1,' and when the signal resonates

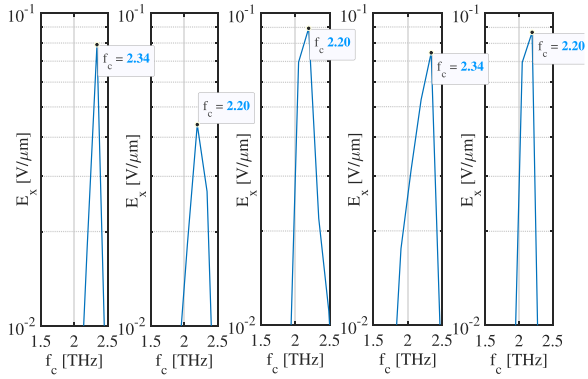

Fig. 9. Frequency spectrum of the THz EM signal in the presence of the modulating gate voltage signal encoded with information bits $M = [10010]$ with a symbol period $T_S = 5$ ps.

at $f_c = 2.20$ THz it is encoded with bit '0'. The modulation bandwidth and modulation depth were calculated as 220 GHz and 3%, respectively, with a frequency deviation of 70 GHz.

V. Conclusion

An efficient transmitter in the THz range is one of the key elements of future high-data-rate wireless networks due to record bandwidths achievable in the THz domain. Among different approaches to the THz signal generation [6], [10], the one based on using plasma oscillations in the 2D electron channel of the graphene HEMT [16], [17], [18], [19], [20], [21], [22], [23], [24], [25], [26], [27], [28], [29] has a number of advantages, such as compact size allowing on-chip integration and room temperature operation. These nanogenerators may be used in many "internet of nano-things" applications like WNoCs, intrabody communications, and wireless nanosensor networks.

Transmission of information in the wireless network requires modulation of the THz carrier signal. Here, we demonstrate successful amplitude and frequency modulation of the THz signal through numerical modeling of the plasmonic graphene HEMT operating in the DS regime. Our simulations show that the signal modulation can be easily achieved using the features of the transistor design. In particular, modulation of the transistor gate voltage with an information signal results in the frequency modulation of the carrier signal. The same modulation of the DC bias current through the transistor yields amplitude modulation of the carrier signal. Modulation bandwidths up to 200 GHz with modulation depths exceeding 75% dependent on the transistor parameters were obtained in our numerical simulations. These results show the possibility of development of the THz nanogenerator with integrated modulator suitable for the wide-ranging applications in communication field.

References

[1] S. Abadal, E. Alarcón, A. Cabellos-Aparicio, M. C. Lemme, and M. Nemirovsky, "Graphene-enabled wireless communication for massive multicore architectures," *IEEE Commun. Mag.*, vol. 51, no. 11, pp. 137–143, Nov. 2013.

[2] I. F. Akyildiz and J. M. Jornet, "The internet of nano-things," *IEEE Wireless Commun.*, vol. 17, no. 6, pp. 58–63, Dec. 2010.

[3] I. F. Akyildiz and J. M. Jornet, "Electromagnetic wireless nanosensor networks," *Nano Commun. Netw.*, vol. 1, no. 1, pp. 3–19, 2010.

[4] S.-B. Lee et al., "A scalable micro wireless interconnect structure for cmps," in *Proc. 15th Annu. Int. Conf. Mobile Comput. Netw.*, 2009, pp. 217–228.

[5] A. Ganguly, K. Chang, S. Deb, P. P. Pande, B. Belzer, and C. Teuscher, "Scalable hybrid wireless network-on-chip architectures for multicore systems," *IEEE Trans. Comput.*, vol. 60, no. 10, pp. 1485–1502, Oct. 2011.

[6] K. Sengupta, T. Nagatsuma, and D. M. Mittleman, "Terahertz integrated electronic and hybrid electronic–photonic systems," *Nature Electron.*, vol. 1, no. 12, pp. 622–635, 2018.

[7] R. Izumi, S. Suzuki, and M. Asada, "1.98 THz resonant-tunneling-diode oscillator with reduced conduction loss by thick antenna electrode," in *Proc. IEEE 42nd Int. Conf. Infrared, Millimeter, Terahertz Waves*, 2017, pp. 1–2.

[8] M. Urteaga, Z. Griffith, M. Seo, J. Hacker, and M. J. Rodwell, "InP HBT technologies for THz integrated circuits," *Proc. IEEE*, vol. 105, no. 6, pp. 1051–1067, Jun. 2017.

[9] A. Maestrini et al., "Frequency tunable electronic sources working at room temperature in the 1 to 3 THz band," in *Terahertz Emitters, Receivers, and Applications III*, vol. 8496. Bellingham, WA, USA: SPIE, 2012, Art. no. 84960F.

[10] P. Shumyatsky and R. R. Alfano, "Terahertz sources," *J. Biomed. Opt.*, vol. 16, no. 3, 2011, Art. no. 033001.

[11] A. Banerjee, L. Zhang, H. Wang, and P. Wambacq, "Sub-THz and THz signal generation using photonic and electronic techniques," in *Proc. IEEE MTT-S Int. Microw. Conf. Hardware Syst. 5G Beyond*, 2019, pp. 1–3.

[12] M. S. Vitiello, L. Consolino, M. Inguscio, and P. De Natale, "Toward new frontiers for terahertz quantum cascade laser frequency combs," *Nanophotonics*, vol. 10, no. 1, pp. 187–194, 2021.

[13] G. Liang, T. Liu, and Q. J. Wang, "Recent developments of terahertz quantum cascade lasers," *IEEE J. Sel. Top. Quantum Electron.*, vol. 23, no. 4, pp. 1–18, Jul./Aug. 2016, Art. no. 1200118.

[14] A. Stohr and D. Jdger, "Photonic millimeter-wave and terahertz source technologies," in *Proc. Int. Topical Meeting Microw. Photon.*, 2006, pp. 1–4.

[15] J. A. Fülöp, S. Tzortzakis, and T. Kampfrath, "Laser-driven strong-field terahertz sources," *Adv. Opt. Mater.*, vol. 8, no. 3, 2020, Art. no. 1900681.

[16] F. Rana, "Graphene terahertz plasmon oscillators," *IEEE Trans. Nanotechnol.*, vol. 7, no. 1, pp. 91–99, Jan. 2008.

[17] V. Ryzhii, T. Otsuji, and M. Shur, "Graphene based plasma-wave devices for terahertz applications," *Appl. Phys. Lett.*, vol. 116, no. 14, 2020, Art. no. 140501.

[18] M. S. Shur and V. Ryzhii, "Plasma wave electronics," *Int. J. High Speed Electron. Syst.*, vol. 13, no. 02, pp. 575–600, 2003.

[19] V. Ryzhii, A. Satou, and T. Otsuji, "Plasma waves in two-dimensional electron-hole system in gated graphene heterostructures," *J. Appl. Phys.*, vol. 101, no. 2, 2007, Art. no. 024509.

[20] M. Shur, G. Aizin, T. Otsuji, and V. Ryzhii, "Plasmonic field-effect transistors (TeraFETs) for 6G communications," *Sensors*, vol. 21, no. 23, 2021, Art. no. 7907.

[21] S. Bhardwaj, N. K. Nahar, S. Rajan, and J. L. Volakis, "Numerical analysis of terahertz emissions from an ungated HEMT using full-wave hydrodynamic model," *IEEE Trans. Electron Devices*, vol. 63, no. 3, pp. 990–996, Mar. 2016.

[22] F. Daneshmandian, A. Abdipour, and A. Askarpour, "Numerical investigation of the instability-based power emission from an ungated plasmonic HEMT using complete hydrodynamic model," *Plasmonics*, vol. 15, no. 6, pp. 1613–1620, 2020.

[23] M. Nafari, G. R. Aizin, and J. M. Jornet, "Plasmonic HEMT terahertz transmitter based on the dyakonov-shur instability: Performance analysis and impact of nonideal boundaries," *Phys. Rev. Appl.*, vol. 10, no. 6, 2018, Art. no. 064025.

[24] V. Popov, O. Polischuk, S. Nikitov, V. Ryzhii, T. Otsuji, and M. Shur, "Amplification and lasing of terahertz radiation by plasmons in graphene with a planar distributed Bragg resonator," *J. Opt.*, vol. 15, no. 11, 2013, Art. no. 114009.

[25] M. Dyakonov and M. Shur, "Shallow water analogy for a ballistic field effect transistor: New mechanism of plasma wave generation by dc current," *Phys. Rev. Lett.*, vol. 71, no. 15, 1993, Art. no. 2465.

[26] J. Crabb, X. Cantos-Roman, J. M. Jornet, and G. R. Aizin, "Hydrodynamic theory of the dyakonov-shur instability in graphene transistors," *Phys. Rev. B*, vol. 104, no. 15, 2021, Art. no. 155440.

[27] D. Yadav et al., "Terahertz light-emitting graphene-channel transistor toward single-mode lasing," *Nanophotonics*, vol. 7, no. 4, pp. 741–752, 2018.

[28] Y. Koseki, V. Ryzhii, T. Otsuji, V. Popov, and A. Satou, "Giant plasmon instability in a dual-grating-gate graphene field-effect transistor," *Phys. Rev. B*, vol. 93, no. 24, 2016, Art. no. 245408.
[29] T. Otsuji et al., "Emission and detection of terahertz radiation using two-dimensional electrons in III–V semiconductors and graphene," *IEEE Trans. THz Sci. Technol.*, vol. 3, no. 1, pp. 63–71, Jan. 2013.
[30] J. M. Jornet and I. F. Akyildiz, "Femtosecond-long pulse-based modulation for terahertz band communication in nanonetworks," *IEEE Trans. Commun.*, vol. 62, no. 5, pp. 1742–1754, May 2014.
[31] M. Rahm, J.-S. Li, and W. J. Padilla, "THz wave modulators: A brief review on different modulation techniques," *J. Infrared Millimeter Terahertz Waves*, vol. 34, no. 1, pp. 1–27, 2013.
[32] A. C. Tasolamprou et al., "Experimental demonstration of ultrafast THz modulation in a graphene-based thin film absorber through negative photoinduced conductivity," *ACS Photon.*, vol. 6, no. 3, pp. 720–727, 2019.
[33] P. K. Singh, G. Aizin, N. Thawdar, M. Medley, and J. M. Jornet, "Graphene-based plasmonic phase modulator for terahertz-band communication," in *Proc. 10th Eur. Conf. Antennas Propag.*, 2016, pp. 1–5.
[34] G. Zhou et al., "Broadband and high modulation-depth THz modulator using low bias controlled VO 2-integrated metasurface," *Opt. Express*, vol. 25, no. 15, pp. 17322–17328, 2017.
[35] Y. Zhang et al., "Large phase modulation of THz wave via an enhanced resonant active HEMT metasurface," *Nanophotonics*, vol. 8, no. 1, pp. 153–170, 2019.
[36] L. Wang et al., "A review of THz modulators with dynamic tunable metasurfaces," *Nanomaterials*, vol. 9, no. 7, 2019, Art. no. 965.
[37] T. Okada and K. Tanaka, "Photo-designed terahertz devices," *Sci. Rep.*, vol. 1, no. 1, pp. 1–5, 2011.
[38] M. Asada and S. Suzuki, "Terahertz emitter using resonant-tunneling diode and applications," *Sensors*, vol. 21, no. 4, 2021, Art. no. 1384.
[39] Y. Ikeda, S. Kitagawa, K. Okada, S. Suzuki, and M. Asada, "Direct intensity modulation of resonant-tunneling-diode terahertz oscillator up to 30 GHz," *IEICE Electron. Express*, vol. 12, no. 3, 2015, Art. no. 20141161.
[40] K. I. Bolotin et al., "Ultrahigh electron mobility in suspended graphene," *Solid State Commun.*, vol. 146, no. 9/10, pp. 351–355, 2008.
[41] L. Banszerus et al., "Ultrahigh-mobility graphene devices from chemical vapor deposition on reusable copper," *Sci. Adv.*, vol. 1, no. 6, 2015, Art. no. e1500222.
[42] J. Crabb, X. Cantos-Roman, G. R. Aizin, and J. M. Jornet, "An on-chip amplitude and frequency modulating graphene-based plasmonic terahertz signal nano-generator," in *Proc. 8th Annu. ACM Int. Conf. Nanoscale Comput. Commun.*, 2021, pp. 1–6.
[43] Q.-T. Vien, M. O. Agyeman, T. A. Le, and T. Mak, "On the nanocommunications at THz band in graphene-enabled wireless network-on-chip," *Math. Problems Eng.*, vol. 2017, 2017.
[44] W. Knap et al., "Terahertz emission by plasma waves in 60 nm gate high electron mobility transistors," *Appl. Phys. Lett.*, vol. 84, no. 13, pp. 2331–2333, 2004.
[45] A. Shabanov et al., "Optimal asymmetry of transistor-based terahertz detectors," *Appl. Phys. Lett.*, vol. 119, no. 16, 2021, Art. no. 163505.
[46] D. Svintsov, V. Vyurkov, V. Ryzhii, and T. Otsuji, "Hydrodynamic electron transport and nonlinear waves in graphene," *Phys. Rev. B*, vol. 88, no. 24, 2013, Art. no. 245444.
[47] C. B. Mendl, M. Polini, and A. Lucas, "Coherent terahertz radiation from a nonlinear oscillator of viscous electrons," *Appl. Phys. Lett.*, vol. 118, no. 1, 2021, Art. no. 013105.
[48] J. M. Jornet and I. F. Akyildiz, "Graphene-based plasmonic nano-antenna for terahertz band communication in nanonetworks," *IEEE J. Sel. Areas Commun.*, vol. 31, no. 12, pp. 685–694, Dec. 2013.
[49] S. Abadal, S. E. Hosseininejad, A. Cabellos-Aparicio, and E. Alarcón, "Graphene-based terahertz antennas for area-constrained applications," in *Proc. 40th Int. Conf. Telecommun. Signal Process.*, 2017, pp. 817–820.
[50] E. Carrasco and J. Perruisseau-Carrier, "Reflectarray antenna at terahertz using graphene," *IEEE Antennas Wireless Propag. Lett.*, vol. 12, pp. 253–256, 2013.
[51] M. Tamagnone, J. Gomez-Diaz, J. R. Mosig, and J. Perruisseau-Carrier, "Reconfigurable terahertz plasmonic antenna concept using a graphene stack," *Appl. Phys. Lett.*, vol. 101, no. 21, 2012, Art. no. 214102.
[52] C. A. Balanis, *Antenna Theory: Analysis and Design*. Hoboken, NJ, USA: Wiley, 2015.
[53] J. Crabb and J. M. Jornet, private communication.
[54] A. Taflove and S. C. Hagness, *Computational Electrodynamics: The Finite-Difference Time-Domain Method*. Norwood, MA, USA: Artech House, 2005.
[55] V. Y. Kachorovskii and M. Shur, "Field effect transistor as ultrafast detector of modulated terahertz radiation," *Solid-State Electron.*, vol. 52, no. 2, pp. 182–185, 2008.

Justin Crabb received the B.S.E.E. degree from the University of Houston, Houston, TX, USA, in 2017, and the M.S.E.E. degree from University at Buffalo, Buffalo, NY, USA, in 2019, with a concentration in telecommunications. He is currently working toward the Ph.D. degree with the Ultrabroadband Nanonetworking Laboratory, Department of Electrical and Computer Engineering, Northeastern University, Boston, MA, USA, under the advisory of Dr. Jornet. His research interests include graphene-based plasmonic THz devices and the development of numerical modeling platforms.

Xavier Cantos-Roman (Student Member, IEEE) received the B.S. degree in telecommunications technologies and services engineering from the Universitat Politècnica de Catalunya, Barcelona, Spain, in 2019. He is currently working toward the Ph.D. degree with Northeastern University, Boston, MA, USA, under the guidance of Dr. Josep M. Jornet. His research interests include the modeling and simulation of THz plasmonic devices, the study of mmWave and THz signals propagation and the design and experimental demonstration of joint communication and sensing systems at sub-THz frequencies. He is a Member of the Ultrabroadband Nanonetworking Laboratory with Northeastern University.

Gregory R. Aizin received the M.S. degree (Hons.) in physics from Belarus State University, Minsk, Belarus, in 1981, and the Ph.D degree in physics from the A. M. Prokhorov Institute of General Physics, Russian Academy of Sciences, Moscow, Russia, in 1986. From 1985 to 1994, he was a Research Scientist with the Institute of Radio engineering and Electronics, Russian Academy of Sciences. From 1994 to 1997 he was a Visiting Research Scholar with Hunter College, New York, NY, USA. Since 1997 he has been a Professor with the Department of Physical Sciences, Kingsborough College, Brooklyn, NY, and Physics Doctoral Faculty with the Graduate School and University Center, City University of New York. His research interests include theoretical studies of transport and collective phenomena in low-dimensional electron systems. His research interests include the theory of interaction of THz electromagnetic radiation with low-dimensional electron systems in semiconductor and graphene nanostructures.

Josep M. Jornet (Senior Member, IEEE) received the B.S. degree in telecommunication engineering, the M.Sc. degree in information and communication technologies from the Universitat Politècnica de Catalunya, Barcelona, Spain, in 2008, and the Ph.D. degree in electrical and computer engineering from the Georgia Institute of Technology, Atlanta, GA, USA, in 2013. Between August 2013 and August 2019, he was a Faculty with the Department of Electrical Engineering, University at Buffalo, Buffalo, NY, USA, and the State University of New York, New York, NY, USA. Since August 2019, he has been an Associate Professor with the Department of Electrical and Computer Engineering, the Director of the Ultrabroadband Nanonetworking Laboratory, and a Member of the Institute for the Wireless Internet of Things at Northeastern University, Boston, MA, USA. In these areas, he has coauthored more than 180 peer-reviewed scientific publications, one book, and has also been granted four US patents. His research interests include terahertz communication networks, wireless nano-bio-communication networks and the Internet of Nano-Things. Since July 2016, he has been the Editor-in-Chief of the *Nano Communication Networks* (Elsevier) Journal. He is the Lead PI on multiple grants from U.S. federal agencies, including the National Science Foundation, Air Force Office of Scientific Research and Air Force Research Laboratory. He is the recipient of the National Science Foundation CAREER award and of several other awards from IEEE, ACM, UB, and NU.